




REGULAR ARTICLE

Enhancement in the Sensing Efficacy of ZnO-based Ethanol Sensor: Fe-ZnO Film

D.K. Chaudhary^{1,*} , S.K. Joshi², S. Thapa³, Y. Yue⁴, P. Zhu⁴

¹ Department of Physics, Amrit Campus, Tribhuvan University, 44600 Kathmandu, Nepal

² Central Department of Chemistry, Tribhuvan University, 44618 Kathmandu, Nepal

³ Department of Physics, Concordia College, Moorhead, MN 56562, USA

⁴ Department of Electrical and Computer Science, University of Missouri, Columbia, MO 65211, USA

(Received 28 December 2023; revised manuscript received 22 April 2024; published online 29 April 2024)

This study compares the gas sensing performance of the ZnO and 5 % Fe-doped ZnO (Fe-ZnO) films synthesized by a spin coating technique. The XRD analysis unveiled the polycrystalline nature of the initially prepared films, showing a decrease in crystallite size from 25.69 ± 0.95 nm for ZnO to 19.49 ± 0.72 nm for Fe-ZnO. Furthermore, the introduction of Fe into ZnO increased the band gap, with values shifting from 3.190 ± 0.105 eV for ZnO to 3.244 ± 0.147 eV for Fe-ZnO and decreased the grain sizes. The reduced grain sizes helped to increase the gas response of the ZnO film. The ethanol vapor sensing experiments performed at a broader temperature range of 100-300 °C demonstrate that the best gas response of the Fe-ZnO film at 260 °C is 17.8 ± 0.4 which was nearly 1.5 times greater than that of the ZnO film at the same temperature. Moreover, it's worth noting that the Fe-ZnO thin film exhibited quicker response and recovery in comparison to the ZnO thin film, with response and recovery times of 32 ± 2 and 162 ± 3 s, accordingly, for 40 ppm ethanol exposure. These findings contribute to a deeper understanding of gas sensing mechanisms in both ZnO and Fe-ZnO thin films which hold promise for future developments in gas sensor technology.

Keywords: Fe-ZnO film, Spin-coating, Surface morphology, Ethanol sensing, Gas response.

DOI: [10.21272/jnep.16\(2\).02011](https://doi.org/10.21272/jnep.16(2).02011)

PACS numbers: 81.20. – n, 78.66. – w,
07.07 – Df

1. INTRODUCTION

Ethanol, a versatile alcohol, holds significant importance across various industries. It serves as a crucial component in pharmaceuticals, solvents, and as a fuel additive [1, 2]. In medicine, it is used as an antiseptic and in the production of vital drugs. Ethanol's role in the beverage industry as an alcoholic beverage is well-known. However, excessive consumption poses serious health risks. It can lead to addiction, liver damage, and impaired cognitive functions. In addition, exposure to ethanol vapor induces ventricular and septal wall stiffening during growth [3]. So, the detection of ethanol vapors is critical for maintaining safety, quality control, and regulatory compliance. Gas sensors play a pivotal role in monitoring ethanol vapors across multiple domains, safeguarding public health and the environment. Having a reliable ethanol sensor is crucial for ensuring safety and precision in various applications. For this, thin films of various types of metal oxide semiconducting materials (MOSm) including, In_2O_3 , Fe_2O_3 , CuO , ZnO and so on emerged as the potential candidates [4-7]. Among various MOSm, ZnO thin films more favorable material for gas sensors due to their non-toxic nature, chemical and thermal stability, tunable surface morphology, electrical, and optical properties which play a vital role in changing their gas sensing properties [7-9].

Generally, ZnO-based ethanol sensors exhibited low

response even at temperatures above 300 °C, which increases power consumption [8, 9]. However, a significant challenge in employing the MOS-based gas sensing technology is to lower the operational temperature while preserving the effective ethanol detection capabilities of ZnO. To overcome this problem, different approaches including metal doping, surface modification, nano-compositing, functionalizing with metallic particles in ZnO, etc., were employed [10, 11], with a recent emphasis on metal doping in ZnO as a solution. As the surface morphology depends on the routes of synthesis, types, and the concentrations of metal-doped into ZnO [10-12], the diverse synthesis methods such as radio frequency sputtering, spray pyrolysis, thermal oxidation, pulse laser deposition, dip coating, hydrothermal, and spin coating are being employed to synthesize the various metals (Fe, Al, Cu, Sn, etc.) doped ZnO films [12-17]. Nonetheless, most of the mentioned synthesis methods necessitate a complex experimental apparatus for achieving the desired quality of ZnO film. Hence, the importance of adopting a straightforward and cost-effective synthesis method that produces high-quality transparent ZnO films, especially with precise control over film thickness, remains paramount in this research field. In this regard, spin coating emerges as a simple, economical approach that optimizes material expenses and time while providing maximum control over film uniformity [18].

With these considerations, this study involved the

* Correspondence e-mail: dinesh.chaudhary@ac.tu.edu.np



synthesis of ZnO and Fe-ZnO films onto glass substrates using the spin-coating method. As-prepared films were employed for ethanol vapor detection at various temperatures. The experimental device employed in this investigation demonstrated its capability to effectively detect ethanol concentrations within the range of 40-400 ppm, all at a specified operating or working temperature of 260 °C. Therefore, this study elucidates the enhancements to the ethanol-sensing properties of ZnO, ultimately leading to the development of an economical gas sensor.

2. EXPERIMENTAL METHOD

2.1 ZnO and Fe-ZnO Film Preparation

Analytical grade chemicals are used for the deposition of the film using a spin coating process on the glass substrate. Prior to depositing the films, the glass substrates were washed with laboline detergent and then cleaned sequentially using acetone and deionized water in an ultrasonic bath. Finally, the substrates were baked in the hot air oven at 60 ± 3 °C for half an hour to get rid of any foreign components.

In the beginning, Zinc acetate di-hydrate was dissolved in ethanol to make 0.35M ZnO precursor solution. Few amounts of di-ethanolamine (DEA) were added to the solution maintaining the same molarity [30]. To make the solution clear and uniform, it was agitated for one hour at (60 ± 5) °C using a magnetic stirrer. The same molar of Fe dopant solution was made by dissolving the ferric nitrate in ethanol in another beaker. These two solutions were further filtered using WHATMAN filter paper. 5% Fe-doped ZnO solutions were obtained by mixing ZnO precursor solution and Fe dopant solution in a ratio of 95:5. The solutions were then aged for 24 hours. The solutions were then coated on cleaned glass substrates using a spin coater. In this process, a few drops of the solution were dropped on the centre of the glass substrate placed on the spin coater. The substrate is then spun rapidly for 10 sec at 500 rpm and for 20 sec at 3000 rpm to spread the coating material. The deposited film was soft baked at (120 ± 5) °C for 5 minutes and then at (450 ± 5) °C for 10 minutes. The coating process was continued multiple cycles until the film reached the required thickness. At the end of multiple coats, ultimately the film was heated at (450 ± 2) °C for 1 hour in the muffle furnace.

2.2 Gas Sensing Setup

The gas sensing efficacy of a prepared ZnO film was measured using a homemade sensing device [Figure 1]. The device was made of an airtight borosilicate glass chamber (height 10 cm, radius 4 cm, and volume 500 ml) with two openings: one for gas in and the other for gas out. The glass chamber is placed on the hot plate. The temperature of the hot plate is controlled by a digital temperature controller (Model: TALBOYS 7X7 CER HP 230 V ADV, manufactured by Troemner, LLC, USA). The ZnO film was placed facing downward inside the chamber at a height of 8 cm from the base of the chamber. A Ni-Cr micro-heater is attached to the back side of the film to heat up to the temperature 400 °C. Its temperature was controlled using the variable power supply. The mean temperature of the test chamber was kept

around the boiling point of the liquid form of analyte gas to stop the formation of liquid of analyte gas. Two electrodes were fabricated on the ZnO film (measuring 2 cm × 1 cm) with a 1 cm separation, using silver paste and copper wire. Subsequently, these electrodes were linked to a multimeter (UNI-T, UT33D+) to quantify their resistance.

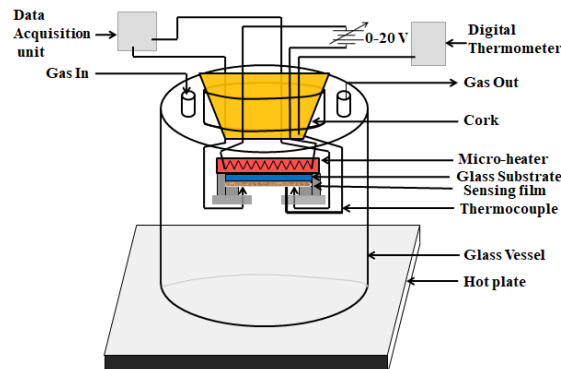


Fig. 1 – Schematic of the gas sensing setup

3. RESULTS AND DISCUSSION

3.1 Structural Properties

Figure 2 depicts the XRD spectra of ZnO and Fe-ZnO films. The intense peaks are observed corresponding to planes (100), (002), (101), (102), (110), (103), (112) etc., indicating the polycrystalline nature of the prepared films. The diffraction peak intensities were less for Fe-ZnO, indicating a decrease in the crystal quality after Fe-doping into ZnO. This is consistent with the published reports [19]. The observed peaks were matched with the JCPDS card numbers 36-1451 to check the purity of the film. A slight shift in the peaks towards a larger angle was found for 5 % Fe-ZnO film. The high-intensity peaks were observed along the (002) plane in the diffraction spectrum of Fe-ZnO, indicating c-axis orientation. The additional impurity phase was not seen.

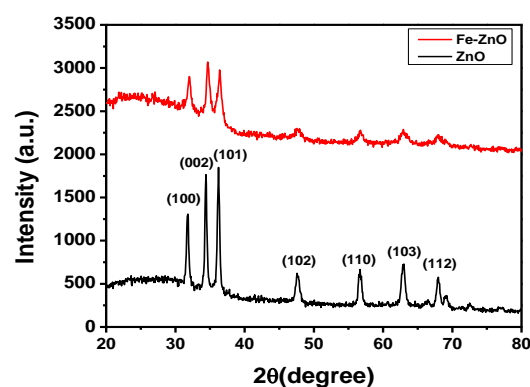


Fig. 2 – X-ray diffraction spectra of ZnO and Fe-ZnO films

Corresponding to the first three major peaks of (100), (002), and (101) planes, the crystallite sizes (D) were determined using Scherer's formula [20]. The mean crystallite size was decreased from 25.69 ± 0.96 nm for ZnO to 19.40 ± 0.72 nm for Fe-ZnO. It is because of the substitution of Zn^{2+} ions (ionic radii, $r_i = 0.74$ Å) by Fe^{2+} and Fe^{3+} ions ($r_i = 0.78$ Å and 0.68 Å respectively) in their lattice

site. The shift in crystallite size causes stresses in the film, resulting in changes in the surface morphology [21].

3.2 Optical Properties

Figure 3(a) depicts the transmission spectra of as-prepared films. The average transmittance decreased slightly from $88.0 \pm 1.2\%$ to $87.7 \pm 1.0\%$ after the addition of Fe into ZnO in the visible range. This decrease in transmittance indicates the oxygen deficiencies in the Fe-ZnO film. The transmittance spectra dramatically decreased in the near UV region because of the absorption. The absorption edge was found at about 355 nm and was shifted towards a shorter wavelength, which is similar to the result reported by Wisz et al., 2017 [22].

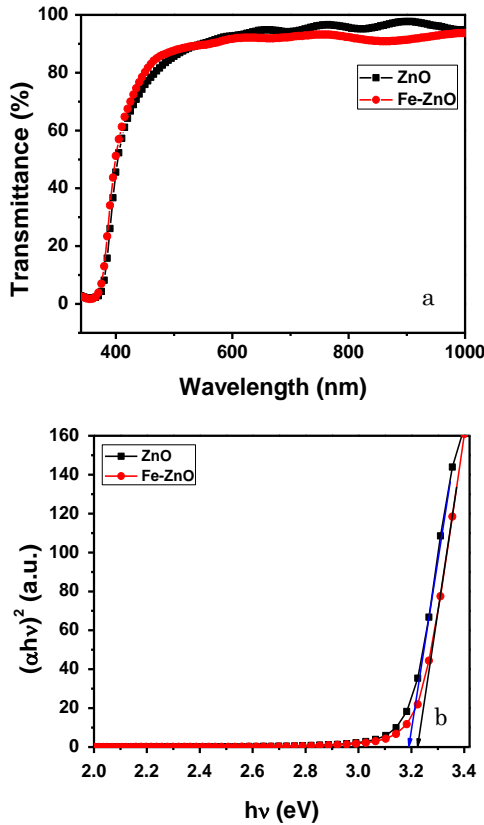


Fig. 3 – (a) Transmittance and (b) Tauc plot of ZnO and Fe-ZnO films

The band gap (E_g) was determined from the Tauc plot [20]:

$$(\alpha h\nu)^2 = A(h\nu - E_g). \quad (1)$$

Here, α – absorption coefficient, A – constant, $h\nu$ – photon energy and E_g – band gap. Through Fe doping, the energy bandgap (E_g) increased from 3.190 ± 0.105 eV in ZnO to 3.224 ± 0.147 eV in Fe-ZnO. This increase in E_g was found to be similar to the published reports [34, 36]. It is because of the replacement of Zn^{2+} ion by Fe^{3+} ion in the lattice site of Zn^{2+} ion which adds the free charge carriers and then shifts the fermi level towards the conduction bands [21].

3.3 Surface Morphology and Elemental Composition

The surface nature or morphology was investigated using scanning electron microscopy (SEM). The SEM images of the films are displayed in Figure 4(a-b). The grain sizes of Fe-ZnO were found to be smaller than that of ZnO. It is because of the substitution of Fe^{2+} and Fe^{3+} ions ($r_i = 0.78 \text{ \AA}$ and 0.68 \AA , respectively) in the lattice site of Zn^{2+} ions ($r_i = 0.74 \text{ \AA}$) which is also supported by the result of XRD. The films' EDX (energy-dispersive X-ray diffraction) spectra are shown in Figure 4(c-d). The EDX analysis reveals distinct peaks for Zn and O exclusively in the ZnO film, and likewise, in the Fe-ZnO film, peaks for Zn, O, and Fe are evident, indicating the pristine nature of the films and the success of the doping of Fe-ions into the native ZnO structure.

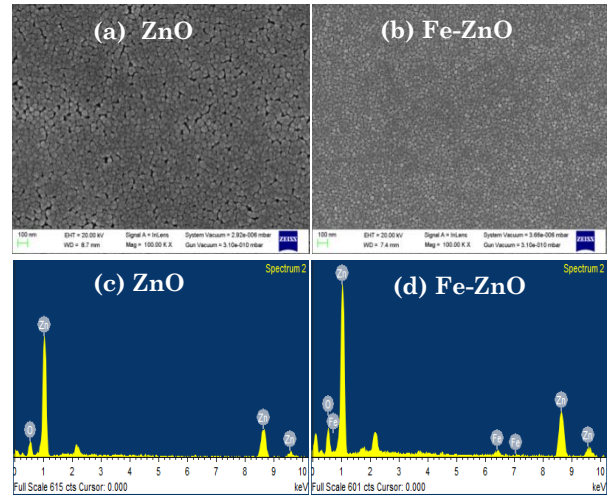


Fig. 4 – (a-b) SEM images and (c-d) EDX spectra of ZnO and Fe-ZnO films

The presence of elements content in these prepared films is shown in Table 1. The findings suggest a reduction in the atomic percentage of oxygen, dropping from 47.67 % in ZnO to 44.82 % in Fe-ZnO. This signifies that the introduction of Fe into ZnO led to an increase in oxygen deficiencies, a conclusion supported by the observed change in the band gap after Fe doping in the optical measurements.

Table 1 – Content of elements in ZnO and Fe-ZnO films

Sample	Elements (at.%)			Total
	Zn	O	Fe	
ZnO	52.33	47.67	–	100
Fe-ZnO	53.03	44.82	2.15	100

3.4 Gas Sensing Properties

In this investigation, the sensing characteristics of the samples were assessed by measuring their resistances in air and gaseous environments and then evaluated the sensing ability in terms of the gas response (R) as:

$$R = \frac{R_a}{R_g}. \quad (2)$$

Here, R_a and R_g are the resistances of samples in air and

gaseous environments [20]. As the gas response of ZnO is temperature dependent, the gas response was measured at the temperature 100-300 °C to determine the optimal working temperature. Figure 5(a) depicts the plot of gas response against the temperature of both ZnO and Fe-ZnO films at 400 ppm ethanol exposure. The gas response increased first with temperature and became highest at a particular temperature of 260 °C, called operating temperature, and then decreased further. The ZnO and Fe-ZnO films exhibited high responses of 12.5 ± 0.3 and 17.8 ± 0.4 at the particular working temperature of 260 °C. It is because the gas response is proportional to the reaction rate coefficient (K_{Eth}) of the molecules of exposed gas with the adsorbed oxygen ions which, in turn, is correlated with the activation energy (E_a) of the barrier of reaction and the absolute temperature as [12, 23]:

$$K_{Eth}(T) = A \exp\left(-\frac{E_a}{k_B T}\right). \quad (3)$$

Here, k_B – Boltzmann constant. The activation energy is the lowest amount of energy needed to activate atoms or molecules for them to participate in a chemical reaction. Thermal energy increases as the temperature rises. When the thermal energy exceeds the activation energy barrier, the charge concentration increases dramatically, resulting in a strong response. If the temperature rises above the optimum, the oxygen ions desorption starts, thereby reducing the gas response [21].

Further, after optimizing the operating temperature, the gas sensing performance of films was extensively investigated at 260 °C. Figure 5(b) depicts the gas response towards 400 ppm of ethanol vapor for 4 cycles.

The sample showed the nearly same responses of ~ 12.5 for ZnO and ~ 17.8 for Fe-ZnO films at 260 °C at each cycle showing the good repeatability of the device.

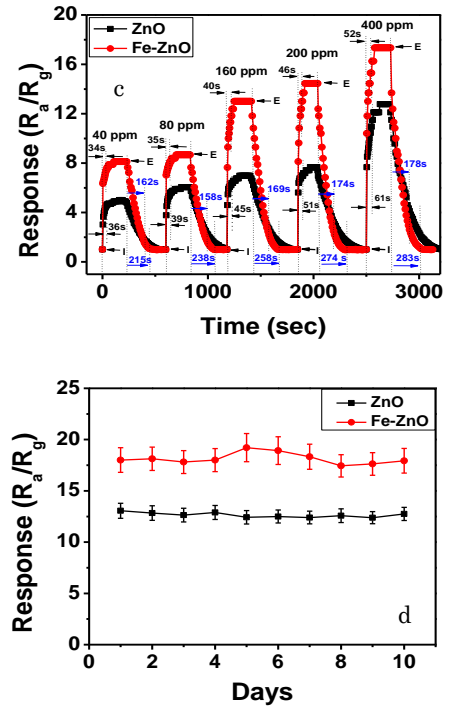
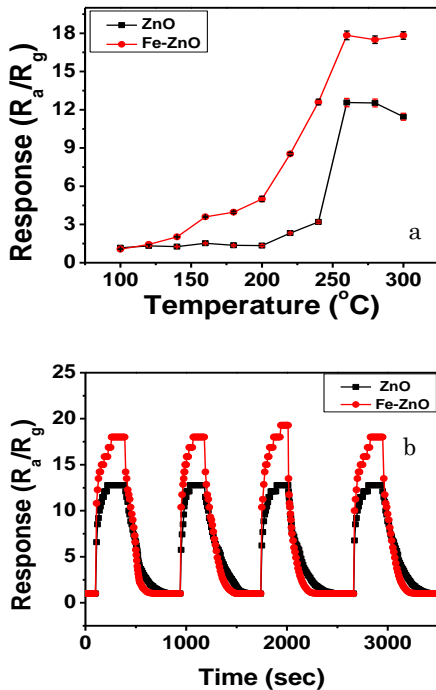


Fig. 5 – (a) Gas response of ZnO and Fe-ZnO thin film at various temperatures for 400 ppm ethanol exposure, (b) repeatability at operating temperature 260 °C for 400 ppm ethanol exposure, (c) response at different concentrations, 40-400 ppm of ethanol, and (d) stability of ZnO and Fe-ZnO sensors

Figure 5(c) depicts the result of the measurement of the gas response for different concentrations of ethanol vapor at 260 °C. This is the plot of gas response with sensing time for different concentrations ranging from 40 to 400 ppm of ethanol vapor. The calculated values of the gas response for different concentrations of ethanol exposure at 260 °C are listed in Table 2. The gas response was increased from 5.0 ± 0.1 to 12.5 ± 0.3 for ZnO and from 8.1 ± 0.2 to 17.8 ± 0.4 for Fe-ZnO. Notably, the Fe-ZnO sample showed a nearly 1.6 time higher response than that of ZnO at 260 °C. There are two reasons for showing the higher response by Fe-ZnO. The higher gas response of Fe-ZnO is due to the smaller grain size of Fe-ZnO than that of ZnO [Figure 3(a-b)] which increased the specific surface area. Moreover, the substitution of Fe^{3+} ions adds the charge carriers which help to adsorb more oxygen to maintain the charge neutrality and hence enhance the gas response [10]. Consequently, extra oxygen ions were adsorbed onto the Fe-ZnO surface and a high response resulted. The two crucial parameters of gas sensors are response time and recovery time. The response time refers to the time needed to reach 90% of maximum response following gas injection into the chamber while the recovery time refers to the time needed to reach the 10% of maximum response following the gas ejection from the chamber. The rate at which the exposed gas interacts with adsorbed oxygen species determines the response time, whereas the rate at which oxygen desorbs from the sensor surface, once the vapor is removed, determines the recovery time. These two parameters are also affected by the sensor setup geometry [20]. Figure Figure 5(c) illustrates the method of calculation of response and recovery times of the ZnO and Fe-

ZnO sensors. The calculated values of gas response, response time, and recovery time are depicted in Table 2. The response and recovery times for ZnO were 61 ± 3 and 283 ± 3 for 400 ppm ethanol exposure whereas those for Fe-ZnO were 52 ± 2 and 178 ± 3 respectively. The Fe-ZnO exhibited a quicker response and recovery than that of ZnO. It may be due to the smaller grain sizes or larger specific area of the Fe-ZnO surface than that of the ZnO surface [Figure 3(a-b)] which helped to increase the oxygen adsorption site and increases the reaction rate of the ethanol molecules with the oxygen ions as well as the adsorption rate of oxygen after the removal of the gas in

the test chamber. To test the stability, the experiments were repeated with similar parameters up to 10 days for 400 ppm ethanol exposure. The gas responses were found to be constant at the value of ~ 12.5 for ZnO and ~ 17.8 for Fe-ZnO showing the consistency of the device across each experiment [Figure 5(d)].

The result of this investigation is also compared to the published reports and found to be better than the published reports. Hence, Fe-doping into ZnO can be utilized to enhance the gas response of the ZnO film-based gas sensors and can be one of the good gas sensors for ethanol detection.

Table 2 – Gas sensing efficacy of ZnO and Fe-ZnO film sensor

Ethanol (ppm)	Undoped ZnO			Fe-ZnO		
	Response (R_a/R_g)	Response time (s)	Recovery time (s)	Response (R_a/R_g)	Response time (s)	Recovery time (s)
40	5.0 ± 0.1	36 ± 2	215 ± 3	8.1 ± 0.2	34 ± 1	162 ± 2
80	6.1 ± 0.2	39 ± 2	238 ± 3	8.7 ± 0.2	35 ± 1	158 ± 2
160	7.0 ± 0.2	45 ± 2	258 ± 3	13.0 ± 0.4	40 ± 2	169 ± 2
200	7.7 ± 0.2	51 ± 3	274 ± 3	14.4 ± 0.5	46 ± 2	174 ± 3
400	12.5 ± 0.3	61 ± 3	283 ± 3	17.8 ± 0.4	52 ± 2	178 ± 3

Table 3 – Comparison of sensing performance of Fe-ZnO sensor in this work with published reports

Sample	Technique	Temperature (°C)	Ethanol Concentration (ppm)	Response (R_a/R_g)	Reference
In ₂ O ₃	Hydrothermal	275	100	11	[4]
α -Fe ₂ O ₃ Nps	Pechini Sol-gel	250	500	11	[5]
CuO	Hydrothermal	300	100	9.1	[6]
ZnO Nps	Co-precipitation	310	100	11	[7]
Al-ZnO	Electro-spinning	250	500	10	[11]
Fe-ZnO	RF sputtering	300	300	2.9	[13]
Al-ZnO	RF sputtering	250	400	20	[14]
Sn-ZnO	Thermal Oxidation Reaction	340	1000	30	[15]
Cu-ZnO	Hydrothermal	200	500	3.2	[16]
Ti-ZnO	Furnace system with hot wire resistance	250	500	2.75	[17]
Sn-ZnO	Low-temperature immersion solution	100	240	3.8	[24]
Fe-ZnO	Spin Coating	260	400 40	17.8 ± 0.4 6.1 ± 0.3	This work

3.5 Gas Sensing Mechanism

The working of a ZnO-based gas sensor can be explained using the classical model in Figure 6. In air, the oxygen molecules come into contact with the ZnO surface. They become adsorbed on the ZnO surface and extract the electrons from the conduction band (CB) of ZnO. Consequently, the adsorbed oxygen molecules are converted into the oxygen ions O⁻, O₂⁻, or O₂²⁻ in accordance with the surface temperature of ZnO. depending on the surface temperature of the ZnO. The adsorption of oxygen molecules and formation of oxygen ions on the ZnO surface are expressed as [23, 24]:

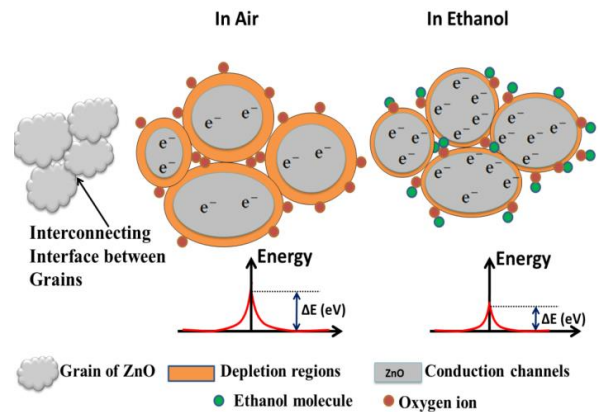
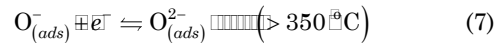
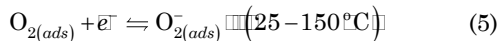
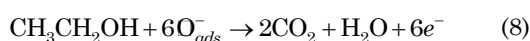


Fig. 6 –Working mechanism of ZnO-based gas sensor

At the temperature of 25-150 °C, O₂⁻ is the predominant species among the adsorbed oxygen ions, which indicates that O₂⁻ ions are primarily adsorbed. As the temperature increases between 150 and 350 °C, the O₂⁻ ions decompose, and the adsorbed species consist of O⁻ and O²⁻ ions. Among these two species, the O⁻ ions become dominant. Finally, when the temperature surpasses 350 °C, O²⁻ ions become more prevalent [39]. Consequently, the width of the space charge layer or depletion layer and the potential barrier height increases, as shown in Figure 6 which increases the ZnO film resistance. At the exposure of ethanol vapor, the adsorbed oxygen interacts with ethanol molecules, releasing electrons back into the ZnO film. This process reduces the potential barrier height and the film resistance. The release of electrons during the interaction of the oxygen ions with ethanol molecules can be explained as follows [13]:



The value of gas response exhibited by the Fe- ZnO film is larger than that of ZnO. The presence of Fe dopant decreases the grain sizes [Figure 3(b)] and increases the specific surface area, leading to the adsorption of additional oxygen ions onto the ZnO surface. Moreover, the Fe dopant adds up extra charge carriers to the ZnO which helps to adsorb the additional number of oxygen to balance the charge neutrality. Thus, when ethanol vapor is exposed to the Fe-ZnO surface, the ethanol molecules interact with the additional number of oxygen ions., thereby releasing the additional number of electrons to the Fe-ZnO surface and enhancing the response.

REFERENCES

1. C. Srinidhi, A. Madhusudhan, S.V. Channapattana, S.V. Gawali, *Heat Transf.* **50**, 2624 (2021).
2. K. Carbone, V. Macchioni, G. Petrella, D.O. Cicero, *Ind. Crops Prod.* **156**, 112888 (2020).
3. K. Kamran, M.Y. Khan, L.A. Minhas, *J. Coll. Physicians Surg. Pak* **19**, 150 (2009).
4. P. Song, D. Han, H. Zhang, J. Li, Z. Yang, Q. Wang, *Sensor. Actuat. B Chem.* **196**, 434 (2014).
5. A. Mirzaei, K. Janghorban, B. Hashemi, M. Bonyani, S.G. Leonardi, G. Neri, *Ceram. Int.* **42**, 6136 (2016).
6. A. Umar, J.-H. Lee, R. Kumar, O. Al-Dossary, A.A. Ibrahim, S. Baskoutas, *Mater. Des.* **105**, 16 (2016).
7. S. Wei, S. Wang, Y. Zhang, M. Zhou, *Sensor. Actuat. B Chem.* **192**, 480 (2014).
8. P. Rai, W.-K. Kwak, Y.-T. Yu, *ACS Appl. Mater. Interfaces* **5**, 3026 (2013).
9. X. Chu, X. Zhu, Y. Dong, X. Ge, S. Zhang, W. Sun, *J. Mater. Sci. Technol.* **28**, 200 (2012).
10. L. Zhu, W. Zeng, *Sensor. Actuat. Phys.* **267**, 242 (2017).
11. M. Zhao, X. Wang, J. Cheng, L. Zhang, J. Jia, X. Li, *Curr. Appl. Phys.* **13**, 403 (2013).
12. A. Khayatian, M.A. Kashi, R. Azimirad, S. Safa, *J. Phys. Appl. Phys.* **47**, 075003 (2014).
13. M.M. Hassan, W. Khan, A.H. Naqvi, P. Mishra, S.S. Islam, *J. Mater. Sci.* **49**, 6248 (2014).
14. S. Chou, L. Teoh, W. Lai, Y. Su, M. Hon, *Sensors* **6**, 1420 (2006).
15. T. Santhaveesuk, S. Choopun, *Adv. Mater. Res.* **770**, 185 (2013).
16. O. Alev, İ. Ergün, O. Özdemir, L.Ç. Arslan, S. Büyükköse, Z.Z. Öztürk, *Mater. Sci. Semicond. Process.* **136**, 106149 (2021).
17. C.-L. Hsu, Y.-D. Gao, Y.-S. Chen, T.-J. Hsueh, *Sensor. Actuat. B Chem.* **192**, 550 (2014).
18. A.P. Rambu, C. Doroftei, L. Ursu, F. Iacomi, *J. Mater. Sci.* **48**, 4305 (2013).
19. C. Liu, D. Meng, H. Pang, X. Wu, J. Xie, X. Yu, L. Chen, X. Liu, *J. Magn. Magn. Mater.* **324**, 3356 (2012).
20. D.K. Chaudhary, M.B. Kshetri, S. Thapa, S.K. Joshi, *Mater. Sci. Forum.* **1074**, 107 (2022).
21. L. Xu, X. Li, *J. Cryst. Growth* **312**, 851 (2010).
22. G. Wisz, I. Virt, P. Sagan, P. Potera, R. Yavorskiy, *Nanoscale Res. Lett.* **12**, 253 (2017).
23. N. Hongsith, E. Wongrat, T. Kerdcharoen, S. Choopun, *Sensor. Actuat. B Chem.* **144**, 67 (2010).
24. R. Mohamed, M.H. Mamat, A.S. Ismail, M.F. Malek, A.S. Zoolfakar, Z. Khusaimi, A.B. Suriani, A. Mohamed, M.K. Ahmad, M. Rusop, *J. Mater. Sci. Mater. Electron.* **28**, 16292 (2017).

4. CONCLUSIONS

In sum, the ZnO and Fe-ZnO films were coated on the glass substrates using an affordable spin coating method that allows for easy control over the thickness of the film. The XRD analysis revealed the polycrystalline wurzite structure of ZnO films in addition to a minor disruption in the microstructure after Fe-doping. XRD and EDX spectra validated the purity of the films. The observed increasing trend of band gap following Fe-doping was consistent with the published reports. The smaller grain sizes of Fe-ZnO demonstrated by SEM images aided in raising the specific surface area and accessible more charge carriers (electrons) due to the substitution of Fe³⁺ ions at the lattice site of Zn²⁺ ion as a key reason for observing increased gas response in Fe-ZnO. The best response achieved with Fe-ZnO was 17.8 ± 0.4 at 400 ppm ethanol with the response and recovery times of 52 ± 2 and 178 ± 3 s, respectively. The gas response found in this work is greater than the some of the published reports. Finally, this work reports that the gas response of a ZnO-based gas sensor can be enhanced by doping Fe into it, which will aid in the fabrication of a cost-effective and efficient ZnO-based sensor for detecting low-concentration ethanol.

ACKNOWLEDGEMENT

The authors are thankful to Indian Institute of Technology (IIT), Roorkee, Uttarakhand, India for SEM, EDX, and XRD experiments.

Підвищення чутливої ефективності датчика етанолу на основі ZnO: плівка Fe-ZnOD.K. Chaudhary¹, S.K. Joshi², S. Thapa³, Y. Yue⁴, P. Zhu⁴¹ *Department of Physics, Amrit Campus, Tribhuvan University, 44600 Kathmandu, Nepal*² *Central Department of Chemistry, Tribhuvan University, 44618 Kathmandu, Nepal*³ *Department of Physics, Concordia College, Moorhead, MN 56562, USA*⁴ *Department of Electrical and Computer Science, University of Missouri, Columbia, MO 65211, USA*

У цьому дослідженні порівнюються характеристики газового зондування плівок ZnO та 5% легованих Fe ZnO (Fe-ZnO), синтезованих методом спінового покриття. Рентгенівський аналіз виявив полікристалічну природу спочатку підготовлених плівок, показавши зменшення розміру кристаліту з $25,69 \pm 0,95$ нм для ZnO до $19,49 \pm 0,72$ нм для Fe-ZnO. Крім того, введення Fe в ZnO збільшило заборонену зону, при цьому значення змістилися з $3,190 \pm 0,105$ eV для ZnO до $3,244 \pm 0,147$ eV для Fe-ZnO і зменшили розміри зерен. Зменшення розмірів зерен сприяло збільшенню газової реакції плівки ZnO. Експерименти з зондуванням парів етанолу, проведені в більш широкому діапазоні температур 100-300oC, показують, що найкраща газова реакція плівки Fe-ZnO при 260 oC становить $17,8 \pm 0,4$, що майже в 1,5 рази більше, ніж у плівки ZnO при тій же температурі. Крім того, варто зазначити, що тонка плівка Fe-ZnO продемонструвала швидшу реакцію та відновлення порівняно з тонкою плівкою ZnO, з часом відгуку та відновлення 32 ± 2 та 162 ± 3 секунди, відповідно, для впливу етанолу 40 ppm. Ці висновки сприяють глибшому розумінню механізмів зондування газу як у тонких плівках ZnO, так і в Fe-ZnO, які є перспективними для майбутніх розробок у технології газових сенсорів.

Ключові слова: Плівка Fe-ZnO, Віджимання, Морфологія поверхні, Зондування етанолу, Газова реакція.